Green Energy and Resources 4 (2026) 100198

Contents lists available at ScienceDirect

Green Energy and Resources

journal homepage: www.journals.elsevier.com/green-energy-and-resources

Research Article

Sulfate resistance of circulating fluidized bed fly ash-based hybrid alkaline cement: Contrasting mechanisms in Na_2SO_4 and $MgSO_4$ environments

Jie Yang[a,b], Tao Meng[a,*], Defu Zhu[a], Fangduo Xiao[a], Xiaoyang Chen[c,*], Jiabin Li[d]

[a] College of Civil Engineering and Architecture, Zhejiang University, Hangzhou, 310058, China
[b] Faculty of Infrastructure Engineering, Dalian University of Technology, Dalian, 116023, China
[c] School of Materials and Metallurgy, University of Science and Technology, Anshan, 114051, China
[d] Research Group RecyCon, Department of Civil Engineering, KU Leuven, Bruges, 8200, Belgium

ARTICLE INFO

Keywords:
Hybrid alkaline cement
Circulating fluidized bed fly ash
Magnesium corrosion
Mechanical properties
Phase composition
Pore structure

ABSTRACT

Traditional cement production remains a significant contributor to CO_2 emissions, therefore, there is a need to explore new types of low-carbon cementitious materials. Hybrid alkaline cement (HAC), a novel cement-based binder with a low carbon footprint, is synthesized from less than 30wt% ordinary Portland cement (OPC) in combination with over 70wt% supplementary cementitious materials. HAC can achieve a shorter setting time and higher mechanical strength than OPC and geopolymer pastes and has been used in rapid construction and repair engineering. However, it remains crucial to determine its suitability for use in saline soil environments. In this study, the adaptability of circulating fluidized bed fly ash (CA)-based HAC (CHAC), OPC and CA-based geopolymer (CG) in the sulfate environment was compared. The temporal and spatial evolution laws of CHAC microstructures in different concentrations of sodium sulfate and magnesium sulfate solutions were elucidated. Results show that the mechanical strength of CHAC can continue to develop even after being immersed in sodium sulfate solution for 120 d, which was 1.39 and 2.62 times greater than that of OPC and CG, respectively. This is because the conversion of C-A-S-H gel into N-A-S-H gel and the crystallization of gypsum optimized the pore structure and densified the matrix of the hardened CHAC. In contrast, $MgSO_4$ exposure produced a distinctly magnesium-driven deterioration process. Mg^{2+} promoted brucite precipitation and the degradation of C-A-S-H gels, generating expansive stress and increasing the total porosity of the CHAC matrix. These coupled effects weakened the matrix and reduced the resistance of CHAC to $MgSO_4$ attack. Nevertheless, CHAC still exhibited higher resistance to magnesium sulfate attack than OPC and CG. These findings confirm that CHAC demonstrates better sulfate resistance compared to OPC and CG, highlighting its potential as a sustainable and durable alternative to traditional cementitious materials.

1. Introduction

Ordinary Portland cement (OPC), the most widely used cementitious material (Bharati et al., 2025), raises significant environmental concerns because of its high CO_2 emissions (Cao et al., 2023; Liu et al., 2022; M. Zhang et al., 2024). Beyond its carbon footprint, the long-term application of OPC in saline or sulfate-bearing environments is also constrained by its phase composition, particularly the presence of reactive aluminate phases and calcium-rich hydration products that can participate in deleterious reactions. These environmental and durability limitations have stimulated increasing interest in alternative cementitious binders with lower clinker consumption and improved adaptability to aggressive service conditions (Zheng et al., 2025).

Hybrid alkaline cement (HAC) has attracted increasing attention as a low-carbon cementitious binder because it combines a small proportion of ordinary Portland cement (OPC, $\leq$30%) with a large fraction of supplementary cementitious materials (SCMs, $\geq$70%) and alkaline activators (Alahrache et al., 2016; Palomo et al., 2007). Compared with OPC, HAC can reduce the clinker content while maintaining rapid setting and high mechanical strength (Lin et al., 2023; Xue et al., 2022). Its performance is mainly governed by the coexistence and interaction of calcium-rich hydration products and alkali-activated aluminosilicate

This article is part of a special issue entitled: Innovative Theories and Technologies for Magnesium Applications in Building Materials and Chemical Engineering Processes published in Green Energy and Resources.

* Corresponding authors.
E-mail addresses: taomeng@zju.edu.cn (T. Meng), askdcxy@126.com (X. Chen).

https://doi.org/10.1016/j.gerr.2026.100198
Received 24 January 2026; Received in revised form 7 June 2026; Accepted 19 June 2026
2949-7205/© 2026 The Authors. Published by Elsevier B.V. on behalf of Shandong University. This is an open access article under the CC BY-NC-ND license (http://creativecommons.org/licenses/by-nc-nd/4.0/).

gels (Xue et al., 2021). Previous studies have shown that C-(A)-S-H and N(C)-A-S-H gels, together with crystalline phases such as ettringite and gypsum, contribute significantly to the strength development of HAC (Xue et al., 2023; Zhou et al., 2024). The reaction degree of SCMs is therefore critical, because reactive silica and alumina can dissolve under alkaline conditions and participate in gel formation, thereby improving the reaction extent, microstructural densification, and mechanical properties of HAC (Liu et al., 2019; Shi et al., 2011). These characteristics indicate that HAC has considerable potential for replacing OPC in low-carbon construction, but its durability in aggressive environments must be clarified before practical application.

Sulfate attack is one of the major deterioration processes affecting cementitious materials in saline soils, groundwater, and marine environments. In OPC-based systems, sulfate ions can react with AFm phases, unhydrated C_3A, and $Ca(OH)_2$ to form ettringite and gypsum, while C-S-H gel may undergo decalcification and decomposition (X. Zhang et al., 2024; Santhanam et al., 2002; Guo et al., 2022). These reactions usually cause expansion, cracking, and strength loss, eventually compromising the integrity of the cementitious matrix (Tian and Cohen, 2000). Geopolymer systems generally exhibit better resistance to Na_2SO_4 attack than OPC because of their lower calcium content and different aluminosilicate gel structure (Komljenović et al., 2013). However, they can still suffer from alkali leaching, microcracks development, and gel degradation during long-term magnesium sulfate exposure (Bakharev et al., 2002). Mg^{2+} can accelerate the decomposition of calcium-bearing gels and promote the formation of expansive or weak reaction products, resulting in more pronounced strength degradation (Bakharev et al., 2002). Therefore, sulfate resistance is strongly dependent on binder chemistry, sulfate cation type, and solution concentration. Although OPC and geopolymers have been widely investigated under sulfate attack, the response of HAC remains less clear because its hybrid reaction products may behave differently from those of either OPC or geopolymers alone.

Circulating fluidized bed fly ash (CA) is a typical industrial by-product generated from boiler combustion, with large annual production but relatively low utilization efficiency (Ge et al., 2022; Li et al., 2018). Compared with conventional fly ash, CA is produced at a lower combustion temperature, generally 850–900°C, which results in relatively low pozzolanic activity when used without treatment (Zhao et al., 2023). Nevertheless, CA contains abundant CaO, SiO_2, Al_2O_3, and SO_3, making it a potentially suitable SCM for HAC preparation. Previous studies have shown that mechanical activation can improve the reactivity of CA, increase the amorphous content, and enhance its activity index and mechanical contribution in cementitious systems (Li et al., 2021; Zhao et al., 2015). Our previous work also demonstrated that CA-based HAC can achieve high mechanical strength when sodium silicate is used as the activator (Yang et al., 2025). These findings suggest that CA has potential for preparing low-carbon HAC and promoting the high-value utilization of industrial solid waste.

However, the sulfate resistance of CA-based HAC remains insufficiently understood, particularly because the high calcium and sulfate contents of CA may strongly affect hydration product evolution, sulfate reaction pathways, and damage mechanisms under external sulfate exposure. Moreover, the distinct effects of sulfate cation type, especially Na_2SO_4 and $MgSO_4$, on the durability of CA-based HAC have not been clarified. Therefore, the durability behavior of CA-based HAC cannot be directly inferred from conventional OPC or geopolymer systems. To address this gap, this study prepared circulating fluidized bed fly ash-based hybrid alkaline cement (CHAC) using CA as the main SCM and compared its strength evolution in 2% and 5% Na_2SO_4 and $MgSO_4$ solutions with those of OPC and CA-based geopolymer (CG). The phase assemblage, microstructure, and pore structure were further analyzed to reveal the sulfate attack mechanism of CA-based HAC, with particular emphasis on the magnesium-driven deterioration process and its feasibility for saline soil applications.

2. Materials and methods

2.1. Materials and mixture proportions

2.1.1. Raw materials

In this study, the OPC with a strength grade of 42.5 was produced by Dalian Cement Group Co., Ltd. The SCM employed was circulating fluidized bed fly ash (CA) sourced from Huadian Electric Power Research Institute Co., Ltd., which was prepared by finely grinding for 60 min using a planetary ball mill and then sieving through a 75-μm square mesh sieve. The chemical compositions of both OPC and CA are presented in Table 1. OPC is primarily composed of CaO and SiO_2, whereas CA mainly consists of CaO, SiO_2, and Al_2O_3. The aggregate used in this study was ISO standard sand obtained from Xiamen Aisino Standard Sand Co., Ltd. All chemical reagents used in the experiments were of analytical grade and were supplied by Tianjin Kemiou Chemical Reagent Co., Ltd. The alkaline activator used was sodium silicate (Na_2SiO_3) particles with a modulus of 1.0.

2.1.2. Specimen preparation

The circulating fluidized bed fly ash-based hybrid alkaline cement (CHAC) mixture proportion was selected based on the low-clinker design principle of HAC and our previous optimization results. A binder composition of 70wt% CA and 30wt% OPC was adopted to reduce OPC consumption while maintaining sufficient calcium availability for hydration and hybrid gel formation. The Na_2SiO_3 dosage of 1.5wt% was chosen because our previous study showed that this activator content produced favorable mechanical performance in CHAC (Yang et al., 2025).

The water-binder ratio was set at 0.5, and the binder-sand was 1:3. This formulation was tested to evaluate the feasibility of CHAC as a cement replacement in terms of sulfate resistance. For comparison, OPC was tested under the same conditions as CHAC.

Additionally, to compare the performance of other cement replacement binders, the circulating fluidized bed fly ash-based geopolymer (CG) was also investigated. Mortars were prepared using 100wt% CA activated with 1.5wt% Na_2SiO_3. The specific mix proportions are presented in Table 2.

In accordance with the mixing procedure in the Chinese National Standard GB/T 17671-2021, water and alkaline activator were first thoroughly mixed and then transferred into the mixing pot. Subsequently, the powder and aggregate were added separately, and the entire mixture was homogenized. The well-mixed paste was then poured into a steel mold with dimensions of 40 mm × 40 mm × 160 mm. After demolding, the specimens were placed in a standard curing environment (temperature 20 ± 2°C, relative humidity ≥95%) for 28 d. Following this curing period, the specimens were removed and immersed in the specified corrosive solution for further testing.

2.1.3. Preparation of attack solution

In this study, solution immersion was selected to provide a controlled and accelerated method for evaluating sulfate attack. Anhydrous sodium sulfate (Na_2SO_4) and anhydrous magnesium sulfate ($MgSO_4$) particles were used as the erosive solutes to prepare sulfate solutions. Based on the concentration (C, %) calculation formula (Eq. (1)), two different concentrations of salt solutions were prepared: 2% and 5%. These concentrations represent low and high sulfate attack environments, respectively.

$$C = \frac{m_e}{m_t + m_e} \times 100\% \quad (1)$$

where m_e is the mass of the solute in grams, and m_t is the mass of the solvent (water) in grams.

Five different immersion solutions were prepared: 2% Na_2SO_4 solution, 5% Na_2SO_4 solution, 2% $MgSO_4$ solution, 5% $MgSO_4$ solution, and

Table 1
Chemical compositions (wt%) of OPC and CA.

Component	CaO	SiO_2	Al_2O_3	SO_3	Fe_2O_3	MgO	K_2O	TiO_2	Na_2O	P_2O_5	Others
OPC	57.72	21.49	7.06	3.86	3.75	3.43	1.25	0.64	0.28	0.07	0.45
CA	29.77	26.64	17.95	14.98	6.06	2.25	0.55	0.94	0.16	0.40	0.30

Table 2
Mixing ratio design of three materials of CHAC, OPC, and CG.

Samples	CA (wt%)	OPC (wt%)	Na_2SiO_3 (wt%)	Water-binder ratio	Binder-sand ratio
CHAC	70	30	1.5	0.5	1:3
OPC	-	100	-		
CG	100	-	1.5		

water. Mortar specimens that had been cured under standard conditions for 28 d were fully immersed in each of these five solutions, ensuring that the specimens in solutions did not come into contact with each other.

To minimize the static characteristics of the experiment, the immersion solutions were replaced on days 1, 3, 7, 14, 28, 56, and 90 of the immersion period. On days 0, 30, 60, 90, and 120 of the immersion process, three specimens of each material were retrieved from each immersion solution for testing.

2.2. Test methods

2.2.1. Mechanical properties

Samples that had been immersed in the corrosive solution for 0, 30, 60, 90, and 120 d were retrieved. The surface moisture of each sample was carefully wiped off. Subsequently, the flexural strength of the samples was tested using the WHY-300/10 universal testing machine, manufactured by Ningbo Saishi Measurement and Control Technology Co., Ltd. For each immersion duration, three specimens were tested, and the average value was calculated and recorded as the flexural strength result. After the flexural strength measurements were completed, the same testing machine was used to assess the compressive strength of six specimens. The average value obtained from these six specimens was designated as the compressive strength result.

2.2.2. XRD analysis

After the strength testing, the fractured samples were soaked in ethanol for 24 h to terminate the hydration process. Subsequently, the samples were vacuum-dried in an oven at 50°C for 24 h to remove residual moisture. The dried samples were then ground into fine powder with a particle size of less than 80 μm using an agate mortar. This powder was analyzed using an X-ray diffractometer (XRD) manufactured by Bruker (model D8 Advance) to analyze the mineral phases of CHAC, OPC, and CG after sulfate attack. The XRD instrument was operated with a Cu target ($\lambda = 0.15418$ nm), at a tube current of 40 mA and a voltage of 40 kV. The scanning range was set from 5° to 80°.

2.2.3. Micro-morphological analysis

Following the strength testing, the fractured samples were soaked in ethanol for 24 h to effectively terminate the hydration process. Subsequently, the samples were vacuum-dried in a drying oven at 50°C to remove any residual moisture. The dried samples were then carefully cut into flat slices with a thickness of 1 mm. These slices were further prepared by applying a platinum (Pt) coating using a sputtering technique to enhance their electrical conductivity and surface quality for subsequent analysis. The surface morphology of the samples was examined using Scanning Electron Microscopy (SEM). Additionally, the elemental composition was analyzed using Energy Dispersive Spectroscopy (EDS).

2.2.4. Pore structure analysis

Following the strength testing, the fractured samples were soaked in ethanol for 24 h to effectively terminate the hydration process. Subsequently, the samples were vacuum-dried in a drying oven at 50°C to remove any residual moisture. The dried samples were then carefully cut into 3–5 mm cubes. Subsequently, mercury intrusion porosimetry (MIP) tests were performed using an Auto Pore IV 9500 instrument (Micromeritics, USA) to characterize the evolution of the pore structure.

3. Results

3.1. Effect of attack solution on compressive strength of mortar

3.1.1. Compressive strength change

Fig. 1 illustrates the compressive strengths of CHAC, OPC, and CG after immersion in water and sulfate solutions. As shown in Fig. 1(a), all samples generally exhibited strength growth in Na_2SO_4 solutions, with CHAC consistently showing the highest strength, followed by OPC and CG. For CHAC, the strength increased rapidly during the first 60 d and reached the maximum value after 120 d, with increases of 24.08% and 26.06% in 2% and 5% Na_2SO_4 solutions, respectively, compared with the unimmersed sample. The maximum compressive strength of CHAC reached 73.14 MPa, which was 1.39 and 2.62 times those of OPC and CG at the same age. The slightly higher strength under 5% Na_2SO_4 indicates that Na_2SO_4 promoted further reaction and matrix densification, confirming the superior resistance of CHAC to Na_2SO_4 attack.

Fig. 1(b) demonstrates the compressive strength evolution of CHAC, OPC, and CG in $MgSO_4$ solutions. CHAC exhibited higher strength than OPC and CG during the first 60 d of immersion. At 2% $MgSO_4$, this advantage was maintained throughout the test, and CHAC retained a compressive strength of 56.00 MPa after 120 d, with only a 3.48% decrease from its initial value. In comparison, OPC decreased by 12.43% to 38.58 MPa, while CG reached only 14.64 MPa. At 5% $MgSO_4$, CHAC showed a more pronounced strength reduction with prolonged immersion. Its strength changed little during the first 30 d but decreased by 9.45% and 26.08% at 60 and 90 d, respectively, indicating accelerated deterioration under high Mg^{2+} concentration. After 120 d, the strength of CHAC was slightly lower than that of OPC by 1.10 MPa, but it remained much higher than that of CG. These results indicate that $MgSO_4$ attack was more detrimental than Na_2SO_4 attack, and high $MgSO_4$ concentration significantly weakened the compressive strength retention of CHAC.

3.1.2. Compressive corrosion resistance coefficient

The strength evolution of cementitious specimens under sulfate immersion involves dual competing mechanisms: (1) sulfate-induced chemical degradation and (2) strength enhancement from ongoing hydration during water curing. To isolate the attack effects of sulfate attack from inherent hydration-driven strength development, this study employs the compressive corrosion resistance coefficient (K). Defined as the ratio of post-corrosion strength to initial strength in non-hydrating conditions, K quantitatively characterizes the authentic sulfate deterioration of CHAC materials by eliminating hydration compensation effects. And the specific calculation formulas are presented in Eq. (2).

$$K = \frac{\sigma_{c(t)}}{\sigma_{Wc(t)}} \tag{2}$$

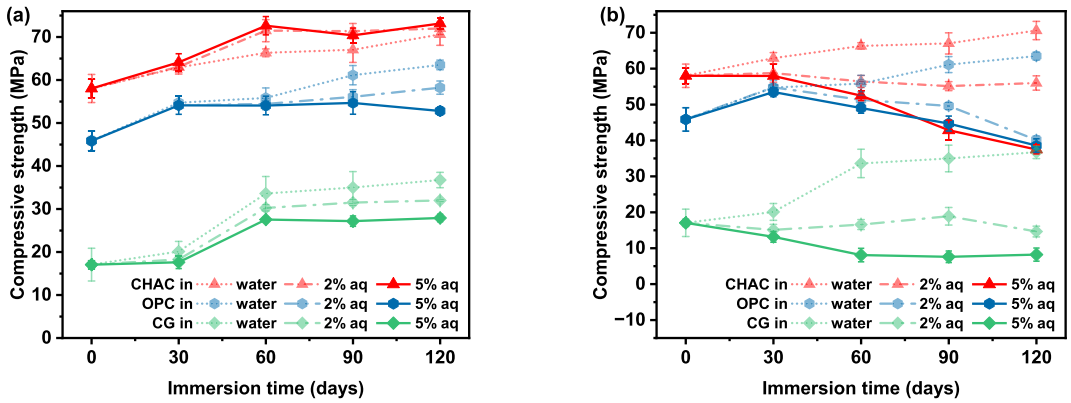


Fig. 1. Compressive strength of samples immersed in solutions: (a) Na_2SO_4, and (b) $MgSO_4$.

where $\sigma_{c(t)}$ represents the compressive strength (MPa) of the specimen after immersion in the sulfate solution for t days; and $\sigma_{Wc(t)}$ denotes the compressive strength (MPa) of the specimen after immersion in water for t days.

Fig. 2(a) and (b) illustrate the evolution of K for CHAC, OPC, and CG in Na_2SO_4 solutions. For CHAC, the K values remained above 1.0 under both 2% and 5% Na_2SO_4 exposure, indicating that Na_2SO_4 immersion enhanced strength development compared with water curing. CHAC consistently showed higher K values than OPC and CG, with maximum values of 1.10 and 1.09 at 60 d in 2% and 5% Na_2SO_4 solutions, respectively. Under 5% Na_2SO_4, the advantage of CHAC became more pronounced with immersion time; at 120 d, its K value was 1.25 and 1.37 times those of OPC and CG, respectively. The slightly higher K values under 5% Na_2SO_4 suggest that increased Na_2SO_4 concentration further promoted the resistance and strength gain of CHAC.

Fig. 2(c) and (d) show the evolution of K for CHAC, OPC, and CG in $MgSO_4$ solutions. Unlike the Na_2SO_4 condition, $MgSO_4$ exposure generally reduced the K values of all binders below 1.0, indicating a clear deterioration effect. In 2% $MgSO_4$, K decreased continuously with immersion time. Although CHAC showed lower K values than OPC at the early stage, it exceeded OPC after 90 d, reaching 1.01 and 1.25 times the OPC values at 90 and 120 d, respectively. CHAC also maintained much higher K values than CG throughout the test. In 5% $MgSO_4$, the decline in K was more pronounced for all samples, confirming the stronger corrosive effect of high-concentration $MgSO_4$. From 30 to 120 d, the K values of CHAC, OPC, and CG decreased by 42.39%, 37.76%, and 66.67%, respectively. These results indicate that $MgSO_4$ attack was significantly more damaging than Na_2SO_4 attack, while CHAC still showed better long-term resistance than CG and comparable performance to OPC.

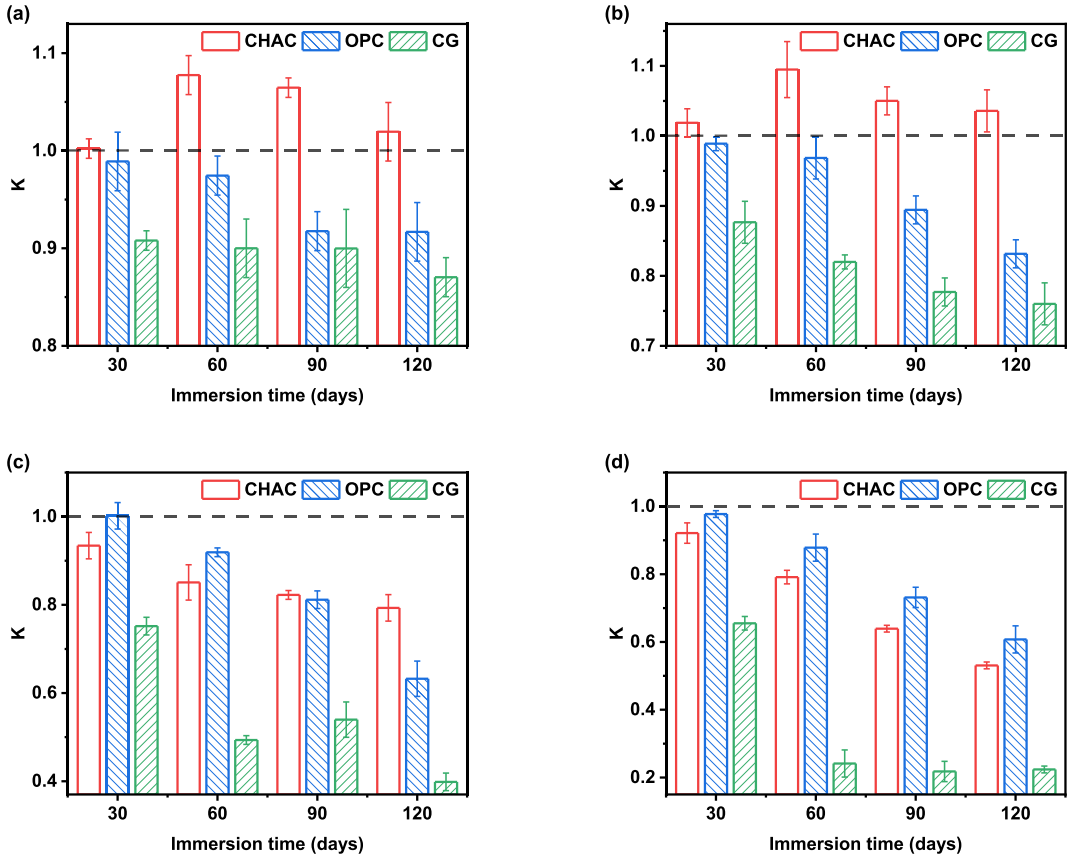


Fig. 2. Change in K of samples immersed in solutions: (a) 2% Na_2SO_4, (b) 5% Na_2SO_4, (c) 2% $MgSO_4$, and (d) 5% $MgSO_4$.

3.2. Effect of attack solution on flexural strength of mortar

3.2.1. Na_2SO_4 attack

Fig. 3(a) presents the flexural strength of CHAC, OPC, and CG after immersion in 2% and 5% Na_2SO_4 solutions for different ages. The flexural strength of CHAC increased with prolonged immersion time, regardless of whether it was immersed in low- or high-concentration Na_2SO_4 solution. After 120 d of immersion, the flexural strength of CHAC increased by 25.7%–30.7% and 19.4%–24.3% compared to its initial value in the low- and high-concentration solutions, respectively. Moreover, the flexural strength of CHAC was consistently higher than that of OPC and CG at the same curing age. After 120 d of immersion, the flexural strength of CHAC was 1.27–1.29 times that of OPC and 3.74–4.13 times that of CG. Additionally, in high-concentration Na_2SO_4 solution, the flexural strength of CHAC at each curing age was higher than that in the low-concentration condition, with the maximum difference reaching up to 1.04 times.

Based on the compressive and flexural strengths of these three materials after 120-d Na_2SO_4 immersion, flexural-to-compressive strength ratios (FCR) were plotted as shown in Fig. 3(b). CHAC demonstrated notable stability in FCR values (0.162–0.183) across both high and low concentration exposures, consistently maintaining intermediate levels between OPC and FG systems. The overall FCR range observed in this study (0.111–0.193) aligns with previous findings (Guo et al., 2020), confirming the characteristic response of cementitious materials to sulfate attack.

3.2.2. $MgSO_4$ attack

The effects of $MgSO_4$ solution concentration and immersion time on the flexural strength of CHAC, OPC, and CG are presented in Fig. 4(a). After 120 d of immersion, the flexural strength of CHAC was higher than that of OPC under the same immersion conditions, with ratios of 1.07 and 1.12 times for low- and high-concentration solutions, respectively. This phenomenon was even more pronounced when compared to CG, where the flexural strength of CHAC under high-concentration immersion was up to 15 times that of CG. The flexural strength of CHAC remains relatively stable, exhibiting a slow, oscillating increase. After 120 d of immersion, the flexural strength of CHAC showed a significant increase compared to its pre-immersion value, reaching 1.04 to 1.09 times the initial strength. During the first 30 d of immersion, an increase in concentration promoted the flexural strength of CHAC. However, after 30 d, the flexural strength of CHAC under high-concentration immersion became significantly lower than that under low-concentration conditions, reaching only 95.45% of the low-concentration value after 120 d.

Fig. 4(b) illustrates the evolution of flexural-to-compressive strength ratio (FCR) for three cementitious materials subjected to $MgSO_4$ attack. Under low-concentration exposure, CHAC exhibited minimal FCR variation, maintaining intermediate values between OPC and CG. Notably, CHAC demonstrated the highest FCR (0.280) under high-concentration attack at 120 d. This phenomenon can be attributed to the differential degradation rates between compressive and flexural strength — while $MgSO_4$ attack caused substantial compressive strength reduction, the flexural strength exhibited comparatively better retention. The measured FCR ranges (0.085–0.281) across all materials align with established literature values (Guo et al., 2020), confirming the validity of our experimental results under MgSO4 exposure conditions.

3.3. Effect of attack solution on mineral composition of mortar

3.3.1. Na_2SO_4 attack

Fig. 5 illustrates the XRD patterns of CHAC immersed in water, 2%, and 5% Na_2SO_4 solutions after 120 d. Due to the high sand content in the raw material and consequently high silica (quartz) content, it is not analyzed in this study as it is not representative. The main hydration products of CHAC were ettringite, gypsum, N-A-S-H, C-S-H, and C-A-S-H (Meng et al., 2025). While water immersion produced more crystalline C-A-S-H, CHAC in Na_2SO_4 solution formed greater amounts of amorphous N-A-S-H gel. However, due to the predominantly amorphous nature of N-A-S-H, its low crystallinity results in weaker XRD diffraction peaks. In addition, CHAC immersed in Na_2SO_4 solution had a higher gypsum content compared to those immersed in water. The production of gypsum and N-A-S-H increased with higher Na_2SO_4 concentrations.

3.3.2. $MgSO_4$ attack

Fig. 6 displays the XRD patterns of CHAC immersed in water and $MgSO_4$ solutions for 120 d. CHAC immersed in $MgSO_4$ solution produced a new hydration product, brucite (Zhang et al., 2011, 2014), compared to CHAC immersed in water. As the concentration of the $MgSO_4$ immersion solution increased, the production of brucite also increased. In addition, the content of C-A-S-H gel in CHAC decreased significantly when the solution concentration was increased. This was analyzed in conjunction with the EDS results and found to be due to the conversion of C-A-S-H to M-A-S-H. However, the latter failed to appear in the XRD patterns, as it is unlikely to exist in a solid solution form (Brew and Glasser, 2005; Lothenbach et al., 2015). The gypsum content of CHAC increased significantly when immersed in high concentrations of $MgSO_4$, which is also one of the products of $MgSO_4$ attack. An increased content of ettringite was generated under high concentration conditions.

3.4. Effect of attack solution on the micromorphology of mortar

3.4.1. Na_2SO_4 attack

The micro-morphology of CHAC before and after immersion in liquid were illustrated in Fig. 7. As shown in Fig. 7(a), the structure of CHAC before immersion was relatively loose, whereas the specimens after

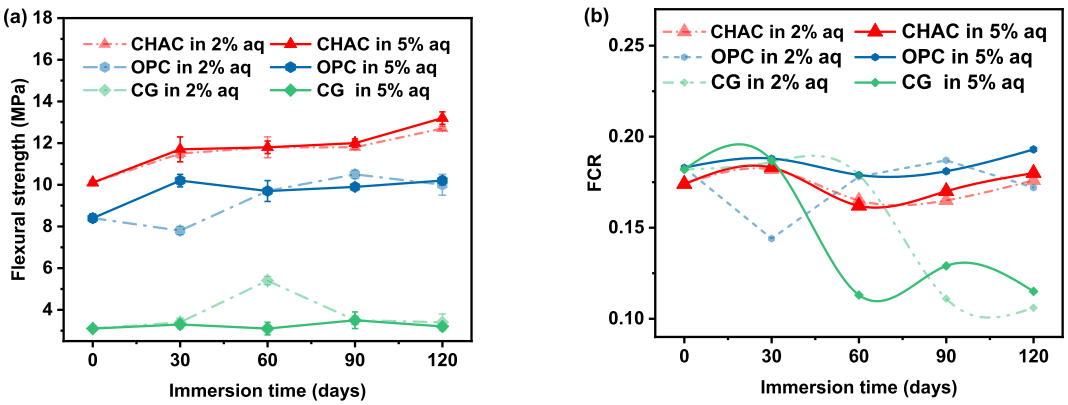


Fig. 3. (a) Flexural strength and (b) FCR of samples immersed in Na_2SO_4 solutions.

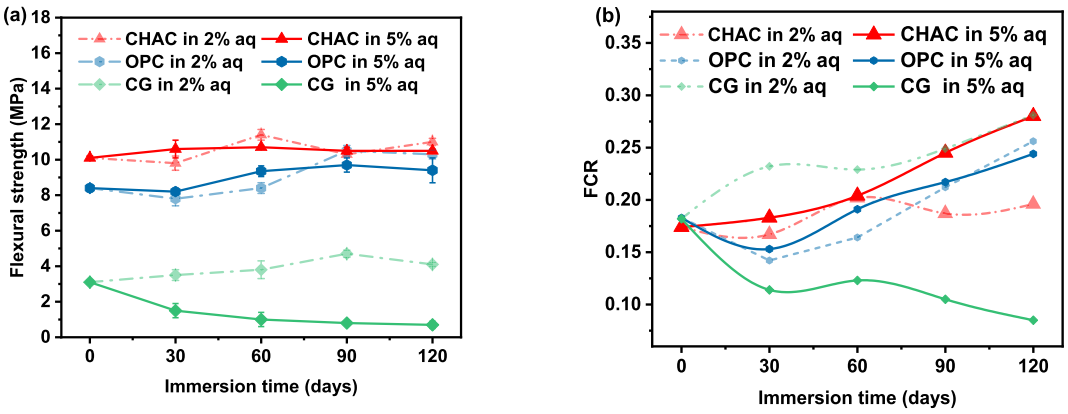


Fig. 4. (a) Flexural strength and (b) FCR of samples immersed in $MgSO_4$ solutions.

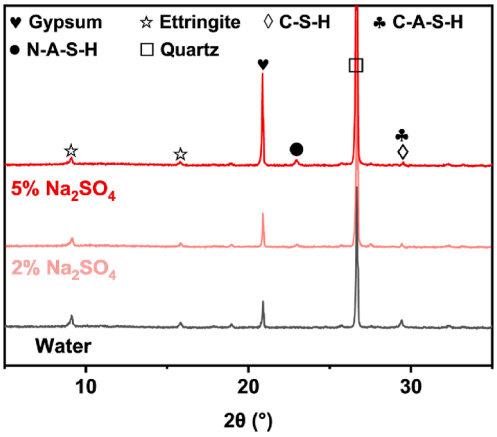


Fig. 5. XRD patterns of CHAC immersed in water and Na_2SO_4 solution for 120 d.

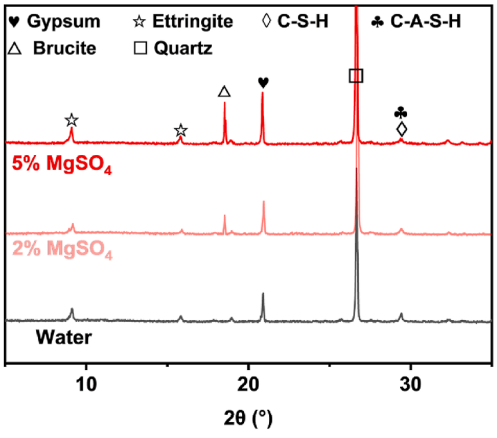


Fig. 6. XRD patterns of CHAC immersed in water and $MgSO_4$ solution for 120 d.

120 d of immersion in both water and Na_2SO_4 solutions exhibited a denser structure (Fig. 7(b)–(d)). In Fig. 7(c), it is observed that coarse rod-like gypsum filled the gaps at the interface between aggregates and cementitious materials, increasing the density of the matrix and making the structure denser. Fig. 7(d) shows that after 120 d of immersion in Na_2SO_4 solution, some of the C-A-S-H gels were transformed into N-A-S-H gels, both of which were interwoven with ettringite to form a complex network structure. This indicates that the hydration products produced after attack by Na_2SO_4 filled the pores within the specimen, reduced the material's porosity, and increased the strength of CHAC. Therefore, CHAC demonstrated good performance in resisting Na_2SO_4 attack. The material avoided corrosion and even enhanced system densification, further verifying its advantage in corrosion resistance.

3.4.2. *$MgSO_4$ attack*

Fig. 8 demonstrates the microscopic morphology of CHAC after 120 d of immersion in $MgSO_4$ solutions. As shown in Fig. 8(a), under the attack of $MgSO_4$, a large number of gels were generated inside CHAC, which EDS confirmed as C-A-S-H and M-A-S-H, respectively. Mg^{2+} in the solution penetrated CHAC through the matrix pores and reacted with the C-A-S-H gel, replacing Ca^{2+} and leading to the formation of M-A-S-H. This process significantly decreased the strength of CHAC. Simultaneously, the generation of brucite by Mg^{2+} in the alkaline environment of CHAC caused cracks to form inside the material, as shown in Fig. 8(b) and (c). These crack provided channels for continuous sulfate ingress into the interior, which is why the material's strength decreases with age. In addition to the above hydration products, scattered gypsum and AFt crystals covering the C-A-S-H gel, as shown in Fig. 8(d), were observed on the surface of the specimens. This observation was in agreement with the results of XRD analysis.

3.5. *Effect of attack solution on pore structure of mortar*

3.5.1. *Na_2SO_4 attack*

The changes in porosity of CHAC under different Na_2SO_4 concentrations and immersion durations are presented in Table 3. As the immersion time increased and the concentration of Na_2SO_4 solution rose, the porosity of CHAC decreased. After 120 d of immersion in low and high concentrations, the porosity of CHAC had decreased by 22.72% and 31.59%, respectively, corresponding to the increase in compressive strength shown in Fig. 1. The pore size distribution of CHAC is illustrated in Fig. 9. When CHAC was immersed in Na_2SO_4 solution, the peak pore size exhibited a significant decrease. As the immersion time extended, the peak pore size continued to gradually decline. After 120 d of immersion, the peak pore size shifted notably to the left (toward a lower diameter). Specifically, it moved from 11.05 nm in the unimmersed state to 5.17 and 4.52 nm in the 2% and 5% concentrations, respectively. This indicated that immersion in Na_2SO_4 refined the pore structure of CHAC, which was consistent with the SEM findings.

Materials are classified into four types of pores based on their diameters: gel pores (<10 nm), transition pores (10–100 nm), capillary pores (100–1000 nm) and macro pores (>1000 nm) (Lv et al., 2024). Fig. 10 characterizes the pore structure evolution of CHAC immersed in Na_2SO_4 solution. After CHAC was immersed in Na_2SO_4 solution, the content of gel pores significantly increased. As the immersion time extended, the gel pore content continued to rise gradually, while the

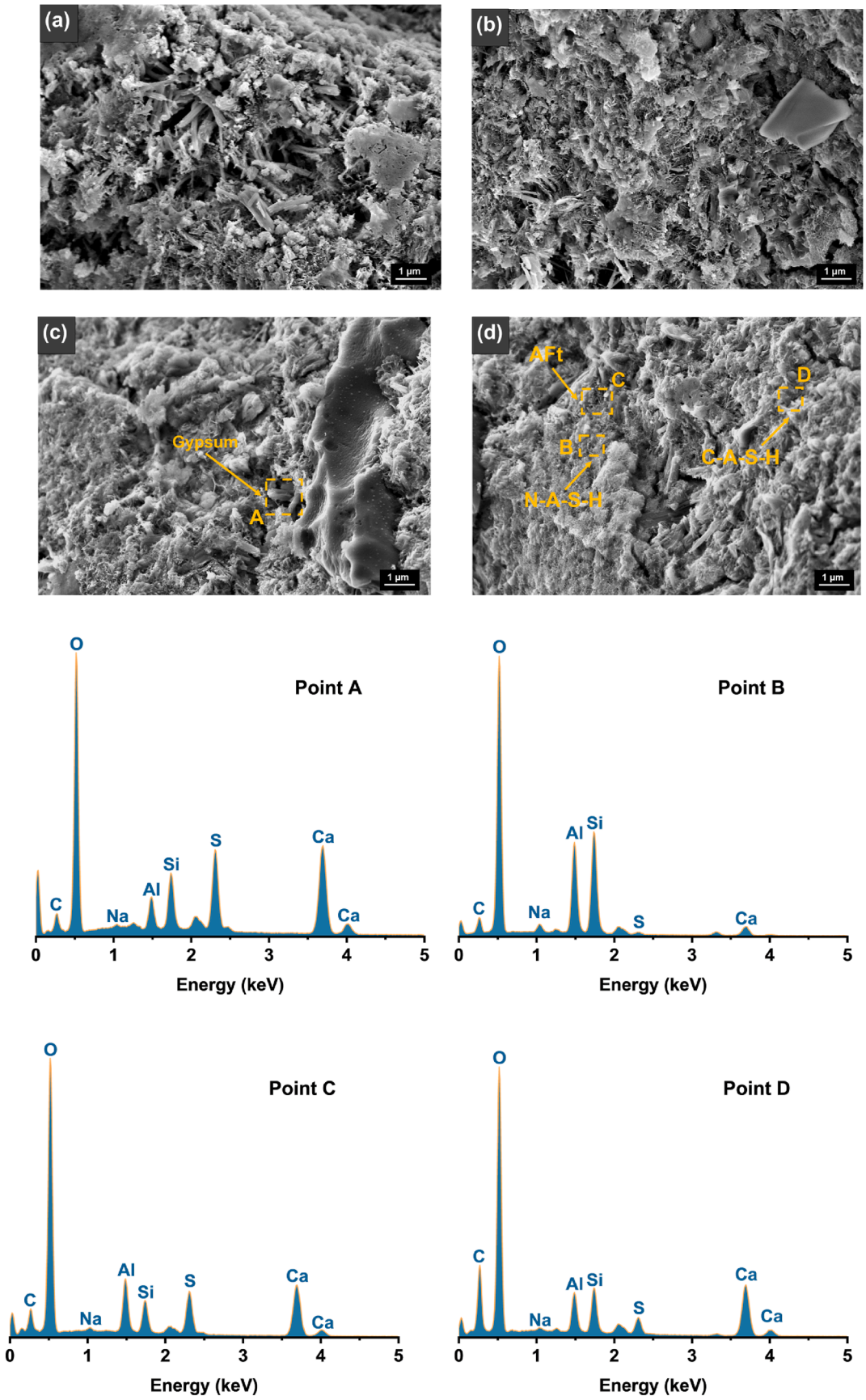


Fig. 7. Microscopic morphology of CHAC under different immersion conditions: (a) before immersion, (b) 120 d in water, (c) 120 d in 2% Na_2SO_4, and (d) 120 d in 5% Na_2SO_4.

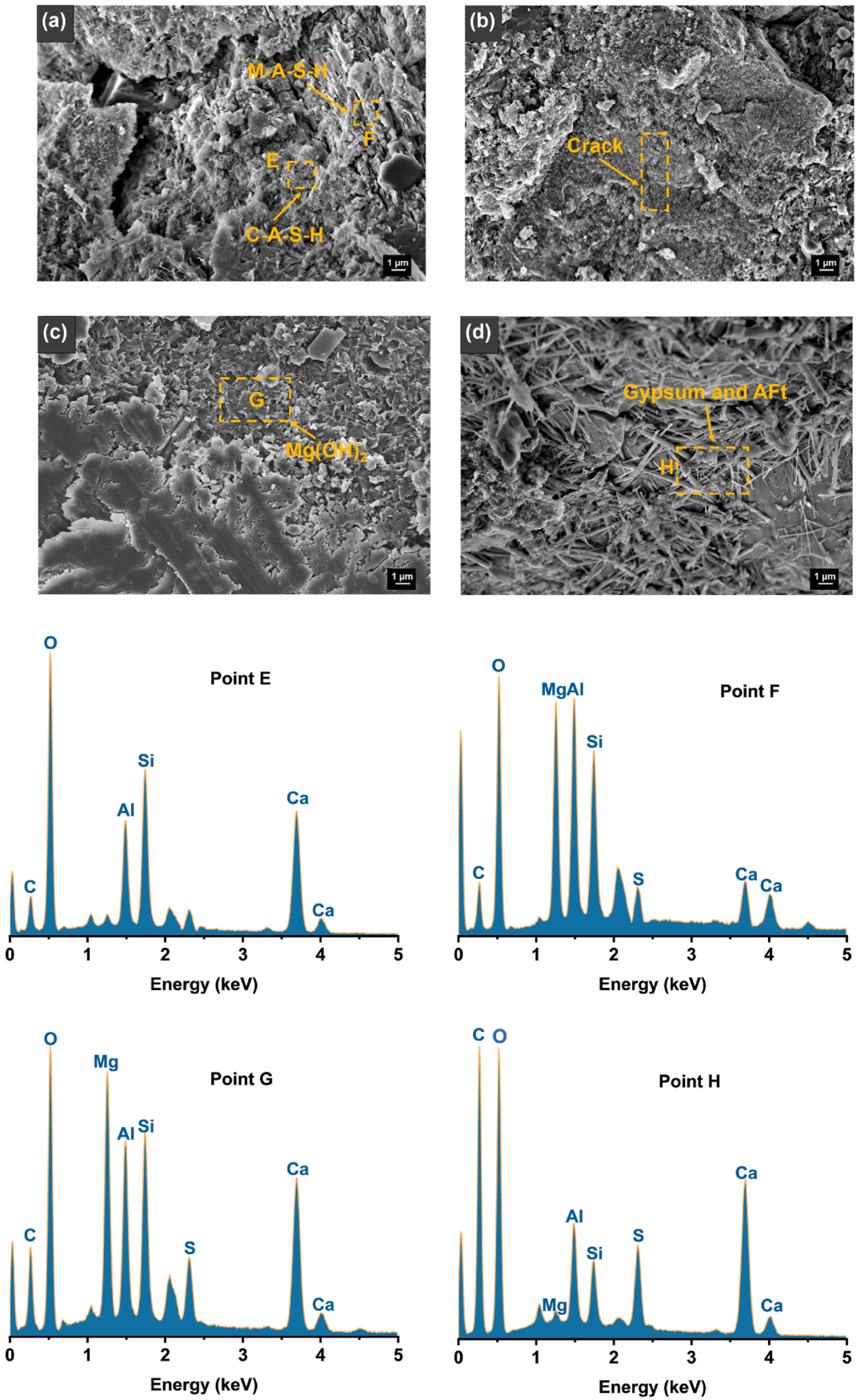


Fig. 8. Microscopic morphology of CHAC immersed in $MgSO_4$ solution for 120 d.

Table 3
Porosity of CHAC immersed in Na_2SO_4 solution at various time.

Concentration (%)	Immersion time (d)	Porosity (%)
2	0	15.45
	30	14.67
	60	13.34
	120	11.94
5	30	13.54
	60	11.05
	120	10.57

macro pore content decreased progressively, indicating that Na_2SO_4 refined the pore structure of CHAC. The increase in Na_2SO_4 concentration further enhanced the gel pore content and reduced the macro pore content, suggesting that the pore-refining effect of Na_2SO_4 on CHAC intensified with higher concentrations. This led to an increase in strength, which is consistent with the conclusions shown in Fig. 1(a).

3.5.2. *$MgSO_4$ attack*

The porosity changes of CHAC after immersion in $MgSO_4$ solution are presented in Table 4. $MgSO_4$ exposure increased the porosity of CHAC, with higher concentrations inducing more significant changes. After 120 d of immersion, the porosity increased by 32.30% and 47.06% at 2% and 5% $MgSO_4$ concentrations, respectively, compared to the pre-immersion state. This trend aligns with the conclusion in Fig. 1(b). Fig. 11 displays the pore size distribution of CHAC immersed in $MgSO_4$ solution over time. After 30 d, a slight increase in peak pore size was observed. This enlargement became more pronounced with prolonged immersion. At lower concentrations, peak migration was less marked, whereas higher concentrations induced more substantial shifts. After 120 d, the peak pore sizes of CHAC reached 12.65 and 13.79 nm under low- and high-concentration conditions, respectively.

Fig. 12 illustrates the pore structure evolution of CHAC under $MgSO_4$ attack. After exposure, CHAC exhibited a significant reduction in gel pores and a corresponding increase in macropores. At lower $MgSO_4$ concentrations, pore redistribution primarily involved interconversion between transition pores and capillary pores, with minimal changes in gel pores and macropores over time. However, at 5% $MgSO_4$ concentration, prolonged erosion progressively transformed gel pores into macropores. This conversion became particularly pronounced after 60 d of immersion, with macropore content increasing by 62.45% and 69.53% at 60 and 120 d, respectively, compared to the pre-immersion state.

Table 4
Porosity of CHAC immersed in $MgSO_4$ solution at various time.

Concentration (%)	Immersion time (d)	Porosity (%)
2	0	15.45
	30	16.01
	60	17.95
	120	20.44
5	30	18.76
	60	19.99
	120	22.72

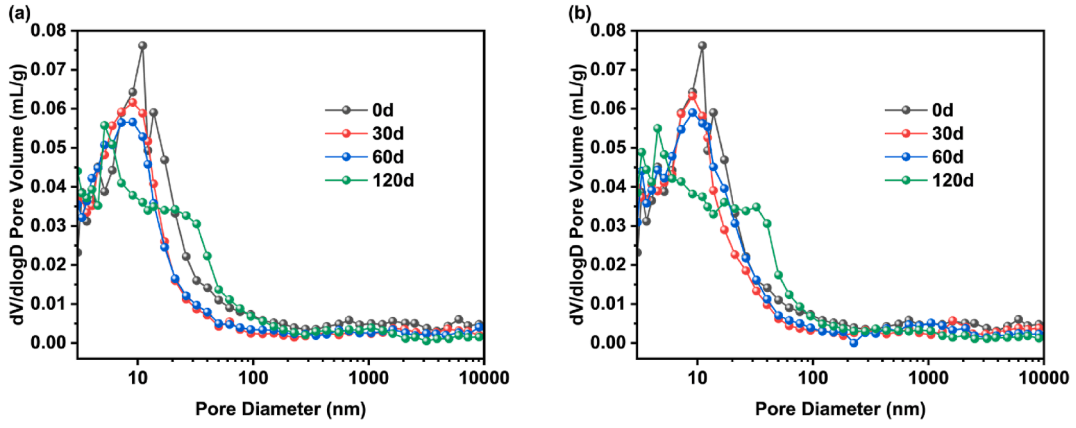


Fig. 9. Pore size distribution of CHAC immersed in Na_2SO_4 solution: (a) 2%, and (b) 5%.

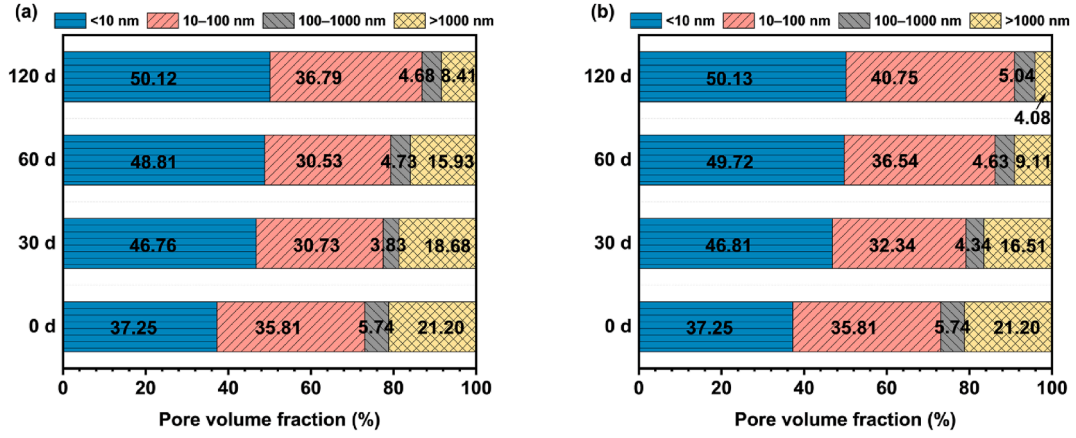


Fig. 10. Pore volume fraction of CHAC immersed in Na_2SO_4 solution: (a) 2%, and (b) 5%.

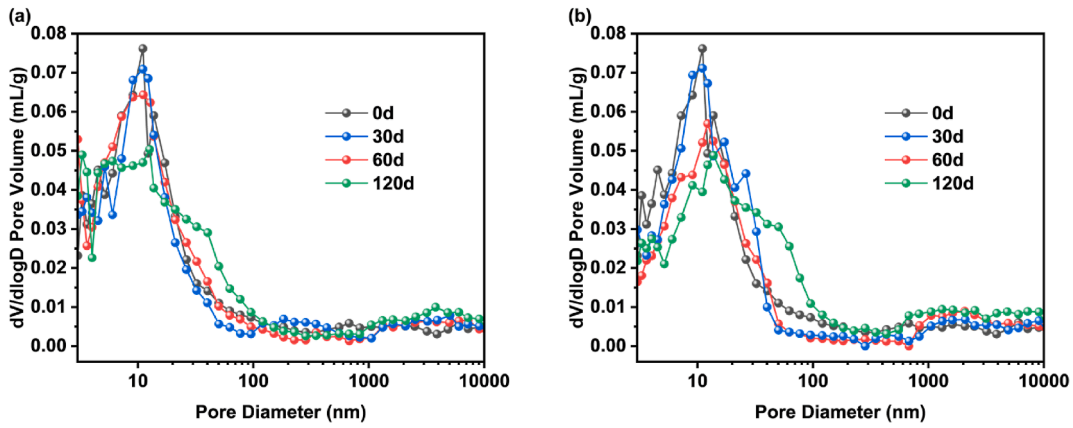


Fig. 11. Pore size distribution of CHAC immersed in $MgSO_4$ solution: (a) 2%, and (b) 5%.

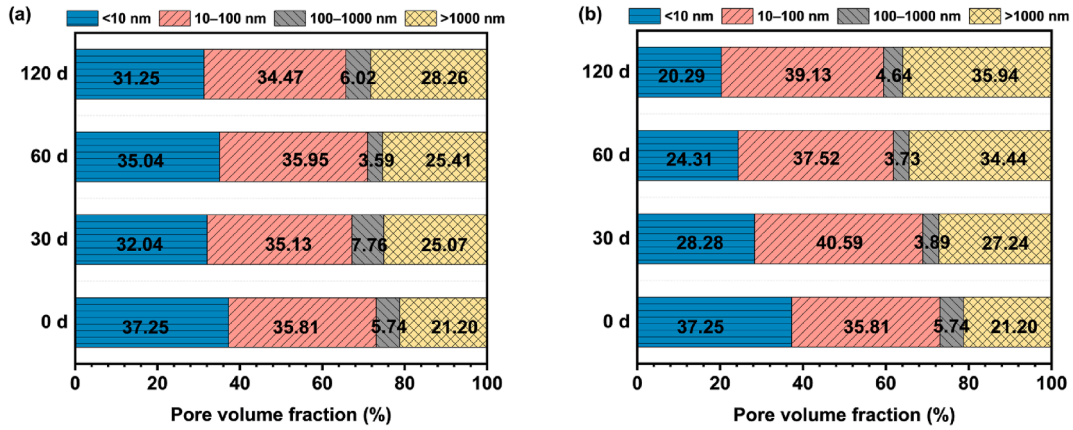


Fig. 12. Pore volume fraction of CHAC immersed in $MgSO_4$ solution: (a) 2%, and (b) 5%.

4. Discussion

4.1. Changes in CHAC strength under sulfate attack

4.1.1. Na_2SO_4 attack

When immersed in Na_2SO_4 solution, the compressive and flexural strengths of CHAC increased with extended immersion time across different concentrations. This indicates that the Na_2SO_4 solution facilitated the hydration of CHAC, promoting the continuous formation of hydration products. The greater the amount of hydration products generated, the faster the strength increase and the better the resistance to Na_2SO_4 attack. And the conclusion was supported by the compressive corrosion resistance coefficient K. During immersion in both high- and low-concentration Na_2SO_4 solutions, the K of CHAC at different ages were all greater than 1.0, indicating that the Na_2SO_4 solution had a more pronounced effect on enhancing CHAC strength than water curing. As the immersion time increased, the rate of increase in mechanical properties also accelerated. This is attributed to Na_2SO_4 acting as an activator, promoting the hydration of CHAC and increasing the amount of reaction products. This indicates that CHAC has excellent resistance to Na_2SO_4 attack, and based on this trend, it can be predicted that the compressive strength of CHAC will continue to grow in the later stages.

In high-concentration Na_2SO_4 solution, the K, compressive and flexural strength of CHAC were generally higher than those in low-concentration solutions, suggesting that higher concentrations of Na_2SO_4 had a more significant promoting effect on the hydration of CHAC. At any immersion time and solution concentration, the compressive strength, K and flexural strength of CHAC exceeded that of OPC and CG, demonstrating that CHAC, as a cement replacement binder, has great potential for resisting Na_2SO_4 attack.

4.1.2. $MgSO_4$ attack

When immersed in low-concentration $MgSO_4$ solution, the compressive strength of CHAC initially increased before decreasing. This trend is primarily due to the rapid strength gain of CHAC in the early stages of immersion, which outpaces the corrosive effects of low-concentration $MgSO_4$. However, as time progresses, the rate of strength gain in CHAC slowed down while the corrosive action of $MgSO_4$ intensifies, ultimately leading to a decline in strength. In contrast, when immersed in high-concentration $MgSO_4$ solution, the compressive strength of CHAC continuously decreased, suggests that the increase in compressive strength at this point was much lower than the corrosive effect of $MgSO_4$. When immersed in low-concentration $MgSO_4$ solution, the compressive and flexural strengths of CHAC were higher than those of OPC and CG, indicating that CHAC had superior resistance to low-concentration $MgSO_4$ attack compared to other materials. Even in high-concentration $MgSO_4$ solution, although the strength of CHAC decreased slightly, it remained significantly higher than that of CG and was either higher than or comparable to OPC.

Overall, the higher the concentration of $MgSO_4$ and the longer the exposure time, the worse the resistance of CHAC to $MgSO_4$ attack. Additionally, CHAC exhibits better resistance to Na_2SO_4 attack than to $MgSO_4$. Therefore, CHAC is recommended for application in saline soils containing Na_2SO_4 or low-concentration $MgSO_4$, but it is not recommended for use in environments with high-concentration $MgSO_4$.

4.2. Mechanism of CHAC against sulfate attack

4.2.1. Mechanism of resistance to Na_2SO_4 attack

As depicted in Fig. 5, after being immersed in Na_2SO_4 solution, the formation of gypsum was distinctly observed under both high- and low-concentration conditions. This occurred because the hydration products of CHAC contained free Ca^{2+}, which reacted with SO_4^{2-} in the solution to form gypsum. On one hand, as shown in Fig. 7(c), the formation of gypsum filled the gaps at the interface between the aggregate and the binder, thereby compacting the matrix and making it denser. On the other hand, the expansion of gypsum reduced the porosity of CHAC by decreasing the size of its pores. As the concentration of Na_2SO_4 increased, the solution provided a greater supply of SO_4^{2-} and Na^+, leading to an increased formation of gypsum. Consequently, higher concentrations of Na_2SO_4 solution had a more pronounced effect on enhancing the strength of CHAC (Wang et al., 2023).

Another mechanism by which Na_2SO_4 enhanced the strength of CHAC was through the formation of N-A-S-H gel, as shown in Fig. 5. C-A-S-H gel is one of the primary hydration products of CHAC and a major contributor to its strength (J. Zhang et al., 2025). When immersed in Na_2SO_4 solution, the free Na^+ in the solution partially replaces Ca+in the C-A-S-H gel due to the ionic radius of the Na^+ being smaller than that of the Ca^{2+}, leading to the formation of N-A-S-H gel. As illustrated in Fig. 7(d), the interwoven network of N-A-S-H gel and C-A-S-H gel filled the pores within the matrix, forming a mesh-like structure that increased the strength of CHAC. Compared to specimens cured in water, those immersed in Na_2SO_4 solution exhibited a greater formation of N-A-S-H gel, with the amount increasing as the solution concentration rose. This was attributed to the continuous supply of Na^+ from Na_2SO_4, which promoted the conversion of C-A-S-H gel to N-A-S-H gel. Higher concentrations of Na_2SO_4 provided more SO_4^{2-} and Na^+ ions to the system, leading to increased formation of both gypsum and N-A-S-H gel in the alkaline environment of CHAC, which is rich in Al^{3+} and Ca^{2+}. This resulted in a denser microstructure with more gel pores and less macro pores due to the filling of pores and the interlocking of hydration products.

In Fig. 5, a slight formation of ettringite was observed in all concentrations of Na_2SO_4 solution. This indicated that the integrity of the hydration product AFt was maintained under both high- and low-concentration Na_2SO_4 attack. The formation of ettringite occurred as SO_4^{2-} from the solution reacted with dissolved Al^{3+} and Ca^{2+} from the reacting CHAC. As shown in Fig. 7(d), the crystalline AFt formed a rigid framework that interlocked with C-A-S-H gel and N-A-S-H gel, creating a dense spatial structure.

The attack mechanism of Na_2SO_4 on CHAC is illustrated in Fig. 13. SO_4^{2-} and Na^+ from the Na_2SO_4 solution penetrated the CHAC matrix and reacted with existing OH^-, Al^{3+}, and Ca^{2+} to form N-A-S-H gel, gypsum, and AFt. The formation of AFt provided a supporting framework, while N-A-S-H gel and gypsum filled the pores of CHAC (Pan et al., 2019). The interlocking of the original C-A-S-H gel with the newly formed N-A-S-H gel under Na_2SO_4 attack enhanced the overall density of the system.

4.2.2. Mechanism of resistance to $MgSO_4$ attack

As shown in Fig. 6, CHAC immersed in $MgSO_4$ solution exhibited the formation of a new hydration product—brucite. This occurred because soluble Mg^{2+} in the solution formed brucite under alkaline conditions (T. Zhang et al., 2025). Since the Ksp of brucite is smaller than that of $Ca(OH)_2$, brucite preferentially precipitates. As the immersion time and concentration of $MgSO_4$ solution increased, excessive formation of brucite progressively depleted available OH^-, lowering the internal pH of CHAC. This led to decalcification and decomposition of C-A-S-H gel, reducing the number of gel pores within the system, the binding properties and strength of CHAC hydration products. Additionally, the formation of Brucite led to expansive damage (Gu and Chen, 2020; Santhanam et al., 2003). The increase in large pores and the generation of cracks further raised the porosity, as shown in Fig. 8(b), Fig. 12(b), and Table 4.

The Ca^{2+} released from decalcified C-A-S-H gel, along with free Ca^{2+} in CHAC, reacted with SO_4^{2-} from $MgSO_4$ to form gypsum (Gu et al., 2021). Gypsum further reacted with C_3A from OPC under alkaline conditions to produce AFt (Liu et al., 2024), with higher concentrations yielding greater amounts. Under low-concentration $MgSO_4$ conditions, the initial formation of gypsum filled internal pores in CHAC, compacting the structure and enhancing strength. However, as $MgSO_4$ concentration increased and immersion time extended, excess SO_4^{2-} led to overproduction of gypsum. Gypsum crystallized and expanded in CHAC, inducing microcracks that accelerated the attack process. Additionally, the increased formation of AFt due to excess gypsum also caused volume expansion, consuming more OH^- and promoting decalcification of C-A-S-H gel. This exacerbated microcracking and strength reduction.

The primary strength source of CHAC is C-A-S-H gel (Zhu et al., 2023). Due to the smaller ionic radius of Mg^{2+} relative to Ca^{2+}, prolonged exposure to high $MgSO_4$ concentrations induced significant decalcification and silicate polymerization in the C-A-S-H, converting it into M-A-S-H. This resulted in a reduction of C-A-S-H and an increase in M-A-S-H, which has a weak cohesive strength, leading to surface erosion and spalling of the degraded layer in the samples (Ye et al., 2019). Consequently, the content of gel pores in CHAC decreased, while the content of large pores increased, leading to a higher porosity. As a result, the strength was reduced. Fig. 14 illustrates the attack mechanism of $MgSO_4$ on CHAC. Mg^{2+} and SO_4^{2-} from the $MgSO_4$ solution penetrated the CHAC matrix. Ca in C-A-S-H gel was replaced by Mg, forming M-A-S-H, loosening the overall structure (Ye et al., 2019). Ca^{2+} released from C-A-S-H gel and free Ca^{2+} in the hydration products reacted with

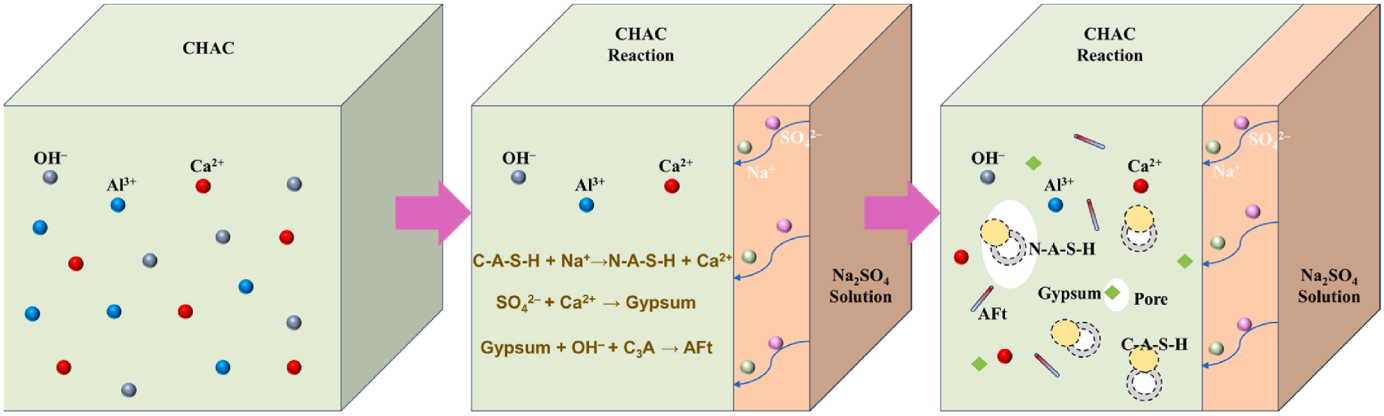


Fig. 13. Reaction mechanism diagram of CHAC attacked by Na_2SO_4.

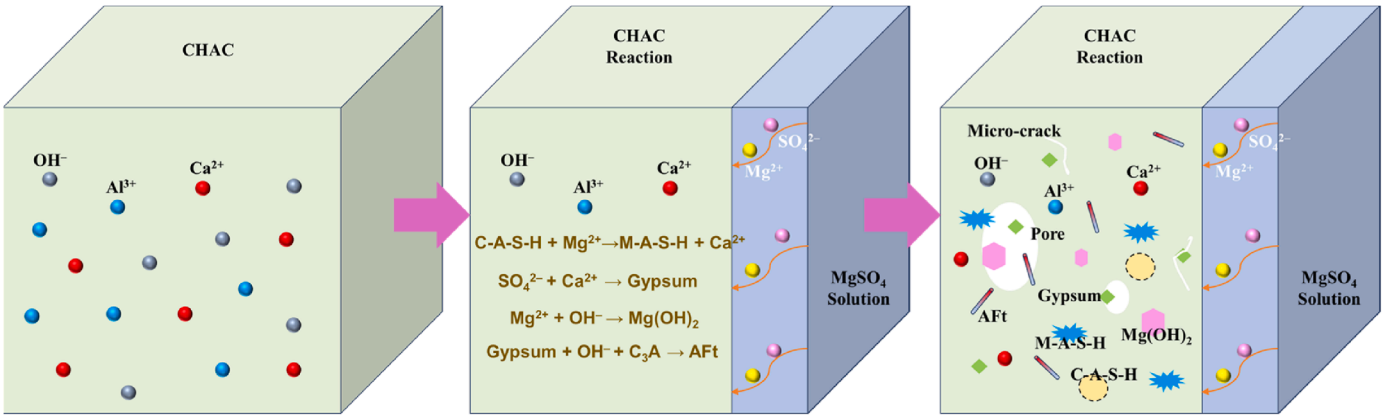


Fig. 14. Reaction mechanism diagram of CHAC attacked by $MgSO_4$.

SO_4^{2-} to form gypsum, which induced microcrack when overproduced. Mg^{2+} formed brucite under alkaline conditions, while gypsum reacted with C_3A from OPC to produce AFt. These reactions caused volume expansion, increased porosity, and ultimately reduced strength.

5. Conclusions

The primary objectives of this study were to elucidate the performance evolution of circulating fluidized bed fly ash-based hybrid alkaline cement (CHAC) under sulfate attack and to clarify the concentration- and cation-dependent reaction mechanisms. Comparative analysis with Ordinary Portland Cement (OPC) and circulating fluidized bed fly ash-based geopolymer (CG) further highlighted the technical superiority of CHAC and its potential to serve as a sustainable cement alternative. Key conclusions are summarized as follows:

(1) CHAC exhibited excellent resistance to Na_2SO_4 attack. Prolonged immersion (120 d) in 2%/5% Na_2SO_4 solutions resulted in progressive enhancement of both compressive and flexural strengths. Microstructural transformation mechanisms involved partial C-A-S-H gel conversion to N-A-S-H phases, and the interlocking network formed by these gels with AFt, along with the pore-filling effect of gypsum, enhanced the density and strength of the CHAC.
(2) The resistance of CHAC to $MgSO_4$ attack was inferior to its resistance to Na_2SO_4 attack. Extended $MgSO_4$ immersion triggered gradual replacement of C-A-S-H by M-A-S-H phases, coupled with brucite-induced pore coarsening that established sulfate diffusion pathways. Accelerated gypsum crystallization ultimately induced localized volumetric stresses and microcrack initiation. Therefore, CHAC can be recommended for Na_2SO_4-type saline soils, but its use in high-concentration $MgSO_4$ environments should be avoided.
(3) CHAC demonstrated superior resistance to sulfate attack compared to OPC and CG. After 120 d of immersion in 2% and 5% Na_2SO_4 and $MgSO_4$ solutions, CHAC maintained higher or comparable compressive and flexural strengths to OPC, indicating its potential as a viable alternative cementitious material.

Herein, this study establishes a compelling case for the large-scale utilization of circulating fluidized bed fly ash in fabricating sulfate-resilient hybrid alkaline cement (HAC). The results demonstrate that CHAC exhibits higher sulfate resistance than OPC and geopolymer.—achieving 120-d compressive strengths of 73.14 MPa in Na_2SO_4 solution (1.39× OPC, 2.62× CG) while maintaining flexural strength superiority (1.27–1.29× OPC, 3.74–4.13× CG). This superior durability, coupled with low-carbon attributes (70% industrial by-product content), positions CHAC as a viable OPC alternative for saline soil engineering applications, such as erosion-resistant foundations, subgrade stabilization, and coastal infrastructure precast elements.

Nevertheless, the dynamic evolution of gel-phase transformation (e.g., C-A-S-H to M-A-S-H under $MgSO_4$ attack) and the spatiotemporal coupling between ion diffusion and microcrack propagation require further exploration. Future work should focus on: (1) Atomic-scale mechanisms of cation exchange (Na^+/Mg^{2+}) in hybrid gels; (2) Long-term (>1 year) performance prediction models integrating pore structure coarsening and brucite-induced expansion; (3) Field validation of CHAC in high-magnesium saline soils to bridge lab-to-practice gaps.

CRediT authorship contribution statement

Jie Yang: Data curation, Methodology, Validation, Visualization, Writing – original draft, Writing – review & editing. **Tao Meng:** Funding acquisition, Supervision, Writing – review & editing. **Defu Zhu:** Data curation. **Fangduo Xiao:** Validation. **Xiaoyang Chen:** Conceptualization, Methodology, Supervision. **Jiabin Li:** Supervision.

Declaration of competing interest

The authors declare that they have no known competing financial interests or personal relationships that could have appeared to influence the work reported in this paper.

Acknowledgements

This work was supported by the National Natural Science Foundation of China (52478282) and the “Pioneer” R&D Program of Zhejiang (2024C04038).

References

Alahrache, S., Winnefeld, F., Champenois, J.-B., Hesselbarth, F., Lothenbach, B., 2016. Chemical activation of hybrid binders based on siliceous fly ash and Portland cement. Cement Concr. Compos. 66, 10–23. https://doi.org/10.1016/j.cemconcomp.2015.11.003.

Bakharev, T., Sanjayan, J.G., Cheng, Y.-B., 2002. Sulfate attack on alkali-activated slag concrete. Cement Concr. Res. 32, 211–216. https://doi.org/10.1016/S0008-8846(01)00659-7.

Bharati, Engelberg, D., Unluer, C., 2025. Characterisation of passive layer on steel immersed in MgO-SiO_2 binder suspension solution. Corros. Sci. 255, 113149. https://doi.org/10.1016/j.corsci.2025.113149.

Brew, D.R.M., Glasser, F.P., 2005. Synthesis and characterisation of magnesium silicate hydrate gels. Cement Concr. Res. 35, 85–98. https://doi.org/10.1016/j.cemconres.2004.06.022.

Cao, Y., Wang, Y., Zhang, Z., Ma, Y., Wang, H., 2023. Thermal stability of limestone calcined clay cement (LC^3) at moderate temperatures 100–400 °C. Cement Concr. Compos. 135, 104832. https://doi.org/10.1016/j.cemconcomp.2022.104832.

Ge, X., Hu, X., Shi, C., 2022. Mechanical properties and microstructure of circulating fluidized bed fly ash and red mud-based geopolymer. Constr. Build. Mater. 340, 127599. https://doi.org/10.1016/j.conbuildmat.2022.127599.

Gu, K., Chen, B., Yu, H., Zhang, N., Bi, W., Guan, Y., 2021. Characterization of magnesium-calcium oxysulfate cement prepared by replacing $MgSO_4$ in magnesium oxysulfate cement with untreated desulfurization gypsum. Cement Concr. Compos. 121, 104091. https://doi.org/10.1016/j.cemconcomp.2021.104091.

Gu, K., Chen, B., 2020. Research on the incorporation of untreated flue gas desulfurization gypsum into magnesium oxysulfate cement. J. Clean. Prod. 271, 122497. https://doi.org/10.1016/j.jclepro.2020.122497.

Guo, L., Wu, Y., Xu, F., Song, X., Ye, J., Duan, P., Zhang, Z., 2020. Sulfate resistance of hybrid fiber reinforced metakaolin geopolymer composites. Compos. B Eng. 183, 107689. https://doi.org/10.1016/j.compositesb.2019.107689.

Guo, Z., Hou, P., Xu, Z., Gao, J., Zhao, Y., 2022. Sulfate attack resistance of tricalcium silicate modified with nano-silica and supplementary cementitious materials. Constr. Build. Mater. 321, 126332. https://doi.org/10.1016/j.conbuildmat.2022.126332.

Komljenović, M., Baščarević, Z., Marjanović, N., Nikolić, V., 2013. External sulfate attack on alkali-activated slag. Constr. Build. Mater. 49, 31–39. https://doi.org/10.1016/j.conbuildmat.2013.08.013.

Li, D., Sun, R., Wang, D., Ren, C., Fang, K., 2021. Study on the pozzolanic activity of ultrafine circulating fluidized-bed fly ash prepared by jet mill. Fuel 291, 120220. https://doi.org/10.1016/j.fuel.2021.120220.

Li, D., Wang, D., Ren, C., Rui, Y., 2018. Investigation of rheological properties of fresh cement paste containing ultrafine circulating fluidized bed fly ash. Constr. Build. Mater. 188, 1007–1013. https://doi.org/10.1016/j.conbuildmat.2018.07.186.

Lin, C., Liu, Z., Gao, Y., Li, Z., Zhang, J., Niu, H., 2023. Study on the effect and mechanism of cement-based material retarder on red mud-based hybrid alkali activated cement. J. Build. Eng. 70, 106353. https://doi.org/10.1016/j.jobe.2023.106353.

Liu, J., Gao, X., Chen, T., 2024. Effect of SiO_2-modified calcined layered double hydroxides on the properties of cement-based material: crucial role of the phase-transformation induced by alkaline pore solution. Cement Concr. Res. 178, 107465. https://doi.org/10.1016/j.cemconres.2024.107465.

Liu, Z., Deng, P., Zhang, Z., 2022. Application of silica-rich biomass ash solid waste in geopolymer preparation: a review. Constr. Build. Mater. 356, 129142. https://doi.org/10.1016/j.conbuildmat.2022.129142.

Liu, Z., Wang, J., Jiang, Q., Cheng, G., Li, Li, Kang, Y., Wang, D., 2019. A green route to sustainable alkali-activated materials by heat and chemical activation of lithium slag. J. Clean. Prod. 225, 1184–1193. https://doi.org/10.1016/j.jclepro.2019.04.018.

Lothenbach, B., Nied, D., L'Hôpital, E., Achiedo, G., Dauzères, A., 2015. Magnesium and calcium silicate hydrates. Cement Concr. Res. 77, 60–68. https://doi.org/10.1016/j.cemconres.2015.06.007.

Lv, T., Zhang, J., Li, C., Xu, L., Hou, D., Hong, S., Dong, B., 2024. Durability and sustainable assessment of fly ash-blended cement paste modified by MgO expansive additive. J. Clean. Prod. 468, 143135. https://doi.org/10.1016/j.jclepro.2024.143135.

Meng, T., Jia, Y., Dai, D., Wang, Z., Lai, J., Lai, Z., Yang, J., He, K., 2025. Effect of nano-$CaCO_3$ on metakaolin geopolymers at different Na/Al ratios: early performance, microstructure, and hydration process. Constr. Build. Mater. 484, 141789. https://doi.org/10.1016/j.conbuildmat.2025.141789.

Palomo, A., Fernández-Jiménez, A., Kovalchuk, G., Ordoñez, L.M., Naranjo, M.C., 2007. Opc-fly ash cementitious systems: study of gel binders produced during alkaline hydration. J. Mater. Sci. 42, 2958–2966. https://doi.org/10.1007/s10853-006-0585-7.

Pan, Z., Wang, S., Liu, Y., Li, B., Jia, Z., Zhang, Y., Wang, J., 2019. The hydration, pore structure and strength of cement-based material prepared with waste soaking solution from acetic acid treatment of regenerated aggregates. J. Clean. Prod. 235, 866–874. https://doi.org/10.1016/j.jclepro.2019.06.335.

Santhanam, M., Cohen, M.D., Olek, J., 2002. Mechanism of sulfate attack: a fresh look part 1: summary of experimental results. Cement Concr. Res. 32, 915–921.

Santhanam, M., Cohen, M.D., Olek, J., 2003. Mechanism of sulfate attack: a fresh look part 2. Proposed mechanisms. Cement Concr. Res. 33, 341–346.

Shi, C., Jiménez, A.F., Palomo, A., 2011. New cements for the 21st century: the pursuit of an alternative to Portland cement. Cement Concr. Res. 41, 750–763. https://doi.org/10.1016/j.cemconres.2011.03.016.

Tian, B., Cohen, M.D., 2000. Does gypsum formation during sulfate attack on concrete lead to expansion? Cement Concr. Res. 30, 117–123. https://doi.org/10.1016/S0008-8846(99)00211-2.

Wang, Y., Cao, Y., Zhang, Z., Zhang, P., Ma, Y., Wang, A., Wang, H., 2023. Intrinsic sulfuric acid resistance of C-(N)-A-S-H and N-A-S-H gels produced by alkali-activation of synthetic calcium aluminosilicate precursors. Cement Concr. Res. 165, 107068. https://doi.org/10.1016/j.cemconres.2022.107068.

Xue, L., Zhang, Z., Liu, H., Jiang, Y., Wang, H., 2022. Drying shrinkage behavior of hybrid alkali activated cement (HAAC) mortars. Constr. Build. Mater. 316, 126068. https://doi.org/10.1016/j.conbuildmat.2021.126068.

Xue, L., Zhang, Z., Walkley, B., Liu, H., Jiang, Y., Wang, H., 2023. Retarding effect of gypsum for hybrid alkali-activated cements (HAACs) at ambient temperature. Mater. Today Commun. 35, 106182. https://doi.org/10.1016/j.mtcomm.2023.106182.

Xue, L., Zhang, Z., Wang, H., 2021. Early hydration kinetics and microstructure development of hybrid alkali activated cements (HAACs) at room temperature. Cement Concr. Compos. 123, 104200. https://doi.org/10.1016/j.cemconcomp.2021.104200.

Yang, J., Meng, T., Han, J., Qiao, Y., Chen, X., Wang, Q., Zhang, T., 2025. Mechanical properties and microstructure of circulating fluidized bed fly ash-based hybrid alkali-activated cement. Constr. Build. Mater. 486, 142006. https://doi.org/10.1016/j.conbuildmat.2025.142006.

Ye, H., Chen, Z., Huang, L., 2019. Mechanism of sulfate attack on alkali-activated slag: the role of activator composition. Cement Concr. Res. 125, 105868. https://doi.org/10.1016/j.cemconres.2019.105868.

Zhang, J., Li, C., Lv, T., Zhao, Q., Dong, B., 2025. Microstructure regulation and performance enhancement of waste gypsum-based supersulfated cement with sintered sludge ash. Constr. Build. Mater. 477, 141358. https://doi.org/10.1016/j.conbuildmat.2025.141358.

Zhang, M., Zhao, Y., Chen, B., 2024. Efflorescence mitigation in fly ash/slag-based geopolymers: the role of precursor composition and proportions, and admixtures. Constr. Build. Mater. 438, 137216. https://doi.org/10.1016/j.conbuildmat.2024.137216.

Zhang, T., Cheeseman, C.R., Vandeperre, L.J., 2011. Development of low pH cement systems forming magnesium silicate hydrate (M-S-H). Cement Concr. Res. 41, 439–442. https://doi.org/10.1016/j.cemconres.2011.01.016.

Zhang, T., Qiao, Y., Yang, J., Chen, X., 2025. Effect of citric acid and urea on the hydration and strength development of magnesium phosphate cement prepared by brucite. Constr. Build. Mater. 485, 141974. https://doi.org/10.1016/j.conbuildmat.2025.141974.

Zhang, T., Vandeperre, L.J., Cheeseman, C.R., 2014. Formation of magnesium silicate hydrate (M-S-H) cement pastes using sodium hexametaphosphate. Cement Concr. Res. 65, 8–14. https://doi.org/10.1016/j.cemconres.2014.07.001.

Zhang, X., Wang, B., Chang, J., 2024. Adsorption behavior and solidification mechanism of Pb(II) on synthetic C-S-H gel with low and high Ca/Si ratios in highly alkaline environments. J. Environ. Chem. Eng. 12, 113871. https://doi.org/10.1016/j.jece.2024.113871.

Zhao, J., Liu, Q., Long, B., Cheng, Z., Wang, H., Wang, D., 2023. Utilization of coal gangue power generation industry by-product CFA in cement: workability, rheological behavior and microstructure of blended cement paste. Fuel 345, 128185. https://doi.org/10.1016/j.fuel.2023.128185.

Zhao, J., Wang, D., Liao, S., 2015. Effect of mechanical grinding on physical and chemical characteristics of circulating fluidized bed fly ash from coal gangue power plant. Constr. Build. Mater. 101, 851–860. https://doi.org/10.1016/j.conbuildmat.2015.10.144.

Zheng, Q., Yang, E., Li, C., Ren, Q., Zhang, H., Song, F., Liu, B., Jiang, Z., 2025. Influence of ultra-fine pozzolanic materials on the self-healing capabilities of ultra-high performance concrete under carbonation conditioning. Cement Concr. Res. 187, 107712. https://doi.org/10.1016/j.cemconres.2024.107712.

Zhou, Y., Zhan, Y., Gao, H., Zhu, R., 2024. Early properties and reaction mechanism of hybrid alkali-activated cements (HAACs). Mater. Today Commun. 41, 110849. https://doi.org/10.1016/j.mtcomm.2024.110849.

Zhu, X., Vandamme, M., Brochard, L., Zhang, Z., Ren, Q., Li, C., He, B., Zhang, H., Zhang, Y., Chen, Q., Jiang, Z., 2023. Nature of aluminates in C-A-S-H: a cryogenic stability insight, an extension of DNA-code rule, and a general structural-chemical formula. Cement Concr. Res. 167, 107131. https://doi.org/10.1016/j.cemconres.2023.107131.